Thermal conductivity of CaO under the conditions of the Earth's interior

Pooja Vyas [1,*] A. B. Patel [2,†] and N. K. Bhatt [1,‡]

[1]*Department of Physics, Maharaja Krishnakumarsinhji Bhavnagar University, Bhavnagar 364001, Gujarat, India*

[2]*Department of Physics and Astronomy, Johns Hopkins University, 3400 N. Charles Street, Baltimore, Maryland 21218, USA*

(Received 28 April 2023; revised 15 October 2023; accepted 30 November 2023; published 3 January 2024)

The thermal conductivity of mantle materials, viz., oxides, perovskites, and silicates, controls the heat balance and thermal evolution of the Earth. We report the pressure (P) and temperature (T) dependence of lattice thermal conductivity of quicklime, an important insulating oxide in the deepest mantle, by employing the phonon anharmonicity added and density functional theory assisted Debye-Callaway (DC) model. The previous [Vyas *et al.*, Phys. Rev. B **107**, 014107 (2023) and Physica B **645**, 414250 (2022)] first-principles calculations that included the anharmonic contribution to the vibrational response were utilized to deduce the input parameters of the DC model, such as the characteristic temperature, the average phonon velocity, and the thermal Grüneisen parameter. In this paper, instead of the conventional Debye temperature, we used a different characteristic temperature (θ) to derive the resistive umklapp phonon scattering rate. The equilibrium value of θ is derived from the second-order volume (V) derivative of the self-consistent plane-wave total energy, whereas the V and T variation of θ is governed by the explicit V,T-dependent Grüneisen parameter. We employed the lowest-order thermodynamic perturbation theory to find an explicit T-dependent thermal gamma and thereby $\theta(V,T)$. The high-P, T lattice thermal conductivity ($K_{\rm lat}$) results for the B2 phase (CsCl structure) of CaO were also computed and compared with those derived using the Boltzmann transport equation (BTE) approach. While the DC model relies on the equation of states and average phonon group velocity, the discrepancy in high-P data suggests that the effect of inflection of the phonon-phonon scattering mechanism with volume is critical. However, the DC model remains successful for the high-T and low-P evaluation of $K_{\rm lat}$, and the calculated results for high-T but zero-pressure ($K_{\rm lat}$) coincides with results based on the BTE approach. Further, we also obtained the radiative part of the thermal conductivity ($K_{\rm rad}$) from the absorption coefficient that was derived within the independent particle approximation and using the Planck function for the blackbody radiation. The computed results at P and T relevant to the Earth's lower mantle and outer core regions suggest that (i) the radiative component $K_{\rm rad}$ remains two to three orders of magnitude smaller compared to the lattice part, and it is negligible; (ii) the B2 phase of CaO is important at the examined P,T plane, and decisively contributes to the heat transport; and (iii) the estimated value (~ 4.9–$8\ \mathrm{W\,m^{-1}\ K^{-1}}$) of $K_{\rm lat}$ at the core-mantle boundary is of the same order of magnitude as that of cubic $CaSiO_3$ perovskite, and $MgSiO_3$ perovskite and bridgmanite along the geotherm.

DOI: 10.1103/PhysRevB.109.014302

I. INTRODUCTION

The thermal conductivities of solids vary theatrically both in magnitude and with temperature from material to material. This is attributed, experimentally, to the sample size of a single crystal, grain sizes for polycrystalline samples, lattice imperfections, dislocations, and theoretically, to anharmonicity offered by the interatomic forces, interactions between the heat carriers and the lattice waves, etc. [1]. The great variety of processes makes thermal transport an interesting area of study both experimentally and theoretically [2]. This nonequilibrium transport property cannot be solved exactly, and an approach based on a combination of perturbation theory and the Boltzmann equation is often required to analyze the microscopic processes that govern heat conduction by carriers and lattice waves. Lattice thermal conductivity ($K_{\rm lat}$) is a primitive physical quantity that determines the heat transport for nonmetals, if not the only one.

The thermal properties in the Earth's deep interior are controlled by $K_{\rm lat}$ of the Earth's mantle and the core. For instance, the $K_{\rm lat}$ and temperature gradient (∇T) of the deepest mantle (D'' layer) determines the heat flow from the core to the mantle. The interface between the molten metallic core and the rocky mantle is the core-mantle boundary (CMB) located at 2890 km depth. Since the mixed convection between mantle and core materials is prohibited due to gravity, heat from the hot Earth's core has been transported by both the conduction and the radiation ($K_{\rm rad}$, radiative thermal conductivity) parts of the thermal conductivity mechanisms at CMB. In metals, thermal conductivity is dominated by electron transport, whereas in insulators such as oxides and silicates, it is dominated by anharmonic phonon transport. At high temperatures, it is believed that the thermal conductivity of mantle minerals, particularly, due to perovskites, has a vital contribution from $K_{\rm rad}$ [3]. The radiative component of total conduction in defect-free material is determined by the material's

*Corresponding author: poojavyas1251995@gmail.com
†amit07patel@gmail.com
‡nkb@mkbhavuni.edu.in, bhattnisarg@hotmail.com

optical response, viz, the absorptivity [4]. Restricting the CMB heat flow, which can be accomplished through the adequate knowledge of total conductivity $K_{\rm tot}(= K_{\rm lat} + K_{\rm rad})$, can help us to understand the dynamic state and the thermal history of both the mantle and the core [5], as well as the relative importance of conduction versus convection above the CMB. The experimental and theoretical estimates of $K_{\rm lat}$ and $K_{\rm rad}$ under the conditions spanning from the lower mantle (LM) to the CMB are challenging because of extreme P and T, ranging from $23 < P < 135$ GPa and $2000 < T \leqslant 4000$ K, respectively. Also, the estimated values for conductivity in the LM condition disperse from 4 to 16 W m^{-1} K^{-1}. This makes the *ab initio* computations for thermal transport properties nontrivial.

CaO or quicklime is an important constituent of the Earth's LM, and it is the base compound for the formation of $CaSiO_3$ perovskite (CaPv). The high-P,T studies of CaO are essential for a better understanding of the Earth's LM and the outer core. However, its high polarizability, anharmonic nature, and high melting temperature (T_M) are the major constraints for theoretical and *in situ* experimental investigations. To account for the anharmonicity in the B1 phase of lime, in our previous work [6] (hereafter, we refer to Ref. [6] as Paper I), we attempted the anharmonic thermal evaluation using the lowest-order thermodynamic perturbation theory (TPT) in conjunction with the density functional theory (DFT) based quasiharmonic (QH) lattice dynamics. Paper I compares the results for high-T thermal properties by employing the projector augmented wave (PAW) potentials within the local density functional (LDA) and generalized gradient approximation, and it was concluded that the PAW+LDA scheme offers a modest amount of anharmonicity up to 3000 K at zero-pressure condition. Later, we [7] (we refer to Ref. [7] as Paper II) employed the same strategy to investigate the structural phase diagram and thermoelastic properties of lime, and concluded that CaO exists in the B1 phase (NaCl structure) only below 23 GPa and 4600 K. At this pressure and temperature, the B1, B2 (CsCl structure), and the liquid phase coexist [7]. In pressure above it, CaO assumes the B2 phase. Paper II also discusses the structural phase transition from a thermoelastic viewpoint and the thermodynamics of the B2 phase of lime along with the high-P melting curve. Thus, for a P, T range relevant to the mantle-core region the B2 phase is equally important. For instance, Paper II proposes that at the CMB, it is the B2 phase that contributes to various physical quantities.

To our knowledge, no studies on the evaluation of $P-T$ dependence of both $K_{\rm lat}$ and $K_{\rm rad}$ are available for quicklime at mantle-core condition. Recently, Ma *et al.* [8] have presented results for the thermal conductivity of alkaline-earth oxides, including the CaO, to 3000 K at ambient pressure and, in pressure, up to 140 GPa but at room temperature (RT) by solving the BTE. On the contrary, ample literature on thermal conductivity is available for $MgSiO_3$ (MgPv) [9–12], and isostructural and isovalent MgO [13–16]. de Koker [13] determined the temperature variation of $K_{\rm lat}$ and also its pressure variation for various isotherms using the Peierls-Boltzmann transport equation via a combination of first-principles molecular dynamics (MD) and lattice dynamics. Tang and Dong [14] have utilized a numerical technique that combines first-principles electronic band structure theory and Peierls-Boltzmann transport theory to predict the $K_{\rm lat}$ of MgO. Imada *et al.* [15] have used the pulsed light heating thermoreflectance technique to study the pressure variation of $K_{\rm lat}$ for MgO. Dalton *et al.* [16] determined the $K_{\rm lat}$ of MgO at high pressure up to 60 GPa and 300 K via the diamond-anvil cells using the time-domain thermoreflectance technique. Zhang *et al.* [3] have predicted the $P-T$ dependence of $K_{\rm lat}$ using the phonon quasiparticle approach (PQA) that is suitable for strongly anharmonic materials like CaPv. The PQA is a hybrid approach combining *ab initio* lattice dynamics and MD simulations, which fully accounts for anharmonic effects. In other words, it treats the phonon anharmonicity to all orders in principle [17]. Zhang *et al.* [3] also carried out experiments using the pulsed light heating thermoreflectance to measure $K_{\rm lat}$ in a laser-heated diamond-anvil cell. Yang *et al.* [18] studied the strain response of thermal conductivity and also determined the RT conductivity of alkaline-earth chalcogenides including CaO.

Several methods exist for the determination of $K_{\rm lat}$, one of which is by estimating the ∇T from the nonequilibrium MD simulations at a given heat current [19,20]. Another approach is based on the Green-Kubo method using the equilibrium MD simulations [21,22]. However, one major downside of these simulations is to deal with a large supercell to consider the finite size effect and a long computation time for better autocorrelation function's convergence. One way to determine $K_{\rm lat}$ is by using the phonon BTE [1]. An exact solution to the BTE is not possible, and we resort to unavoidable approximations. Though its linearized version is simple and comprises a set of linear equations, the linear equation set has a large dimension. The lack of reliable linear coefficients determined by the interatomic potentials can also make the exact solution of the BTE not so readily available. As a substitute, one can use the DC model [17,23,24] to compute relaxation times. The DC model is believed to operate at the same level of approximations [8,24] as the various other approaches that are used to factorize the set of the linear equation for solving the BTE. Furthermore, it is computationally affordable and resorts to the relaxation time approximation (RTA). Conventionally, the DC model neglects the full phonon dispersion and assumes the phonon density of state (P-DOS) to vary as ω^2. This is true when only low-frequency (ω) acoustic phonons contribute to heat transport. If required, the contribution from the optical modes was included using the single-frequency Einstein model [22]. We have demonstrated in Papers I and II [6,7] that the role of optical phonons is non-negligible for CaO, and they contribute to bonding and other physical properties decisively.

In this paper, we compute the $P-T$ variation of $K_{\rm lat}$ and $K_{\rm rad}$ of lime for both B1 and B2 phases. The computation of $K_{\rm lat}$ is carried out employing the frequently used DC model [23]. However, the ingredients of the DC model, as elaborated in the next section, are derived differently. For insulating materials like CaO, the thermal transport is largely governed by the three-phonon umklapp interactions, which are also responsible for the thermal expansion mechanism. To obtain the anharmonicity-assisted equilibrium volume at each temperature, $V_0(T)$, the total Helmholtz free energy versus volume curve at all temperatures for both phases was computed in

Papers I and II, respectively. The computed $V_0(T)$'s are used in the present paper to evaluate the transport properties. We propose a couple of modifications for computing the model input parameters. In this anharmonicity-included DC model, the relaxation time due to the phonon-phonon scattering can be written as an explicit function of volume (V) and T-dependent characteristic temperature (θ), phonon velocity (v), and the Grüneisen parameter (γ), which are all extracted from the first-principles calculations by optimizing the Helmholtz free energy [6,7]. In this paper, we utilized an explicit T-dependent Grüneisen parameter, and a different characteristic temperature is used instead of the Debye temperature. The pressure variation of the $K_{\rm lat}$ for chosen temperatures is also determined using the BTE approach [1] for the B2 phase of CaO, and computed results are compared and discussed with DC-model based findings. The evaluation of $K_{\rm rad}$ is carried out using a conventional approach [4,25] which involves the computation of the absorption coefficient (α) and the Planck function but now derived at each equilibrium volume $V_0(T)$.

The rest of the paper is organized as follows. In Sec. II, the theory and computational details are elaborated for the evaluation of $K_{\rm lat}$ and $K_{\rm rad}$. The computed results are compared in Sec. III and is followed by a summary, Sec. IV. The paper is concluded in Sec. V.

II. THEORY AND COMPUTATIONAL DETAILS

Previous studies on CaO [6,7,26,27] show the inadequacy of QH approximation in investigating the high-T thermodynamic and structural properties because of its highly polarizable nature and anharmonic interaction present even at RT. Thus, for a reliable study aiming at high-T transport properties, one is required to include an anharmonic contribution using an appropriate theoretical model. As discussed earlier, in Papers I and II, we have utilized the lowest-order TPT to estimate these anharmonic phonon contributions in combination with the DFT based QH phonon dynamics for unveiling the high-P,T behavior of the B1 and B2 phases of CaO. We refer to Papers I and II for complete details about the anharmonic computations for free energy. It was concluded in Papers I and II that anharmonicity in CaO is modest with the PAW+LDA scheme. The equilibrium volume corresponding to each temperature, $V_0(T)$, obtained by minimizing the total (including the anharmonic contribution) Helmholtz free energy for both the phases is utilized for the computation of $K_{\rm lat}$ and $K_{\rm rad}$.

Components of the thermal conductivity tensor can be expressed as a sum over all wave vectors $\vec{k}$ of the first Brillouin zone for each polarization branch ζ,

$$K_{ij} = \sum_{\vec{k},\zeta} v_i(\vec{k}) v_j(\vec{k}) \tau_j C_\zeta . \tag{1}$$

Here, τ_j and C_ζ denote the phonon relaxation time and mode heat capacity per unit volume, respectively. The $v_i(\vec{k})$ represents wave vector dependent phonon velocity. The optical phonons are usually less effective (but not negligible) to carry thermal energy, and are responsible for the attenuation of heat flux originated by the acoustic modes in insulators. Thus, the thermal energy in insulators is carried by acoustic phonons with damping introduced by optical branches of the phonon dispersion curve (PDC). It is then natural to cast the computation of lattice conductivity for the acoustic branch but with a supplement from the high-frequency optical phonons. For weak anharmonic insulating oxides, such as CaO [6,7], the acoustic modes transfer the heat by three-phonon interactions [28,29]. It is argued that the lifetimes of optic modes are considerably shorter than the acoustic modes, and the lattice conductivities are predominantly governed by the acoustic phonons at all pressures studied in the paper [13]. The $K_{\rm lat}$ has three contributions: one from the longitudinal acoustic (K_{LA}) phonon branch and two from the transverse acoustic (K_{TA} and $K_{TA}^{'}$) branches,

$$K_{\rm lat} = K_{LA} + K_{TA} + K'_{TA}. \tag{2}$$

In the RTA, the thermal conductivity is a function of the relaxation time ($\tau_{\rm tot}$), which indicates the time taken by the phonon distribution to restore the equilibrium phonon state. The umklapp process (U process) gives rise to thermal resistance due to the reversed phonon flux, whereas the normal process (N process) considers the redistribution of momentum and energy among phonons. In the DC model, it is assumed that the different scattering mechanisms act independently. For a defect-free crystal, the total phonon scattering rate $\tau_{\rm tot}^{-1}$, which involves the contribution from normal τ_N^{-1} and umklapp τ_U^{-1} scattering processes, can be written as

$$\frac{1}{\tau_{\rm tot}} = \frac{1}{\tau_N} + \frac{1}{\tau_U}. \tag{3}$$

Further, the assumptions made are the following: (i) an average phonon velocity (v) is used for all-optical and acoustic phonon branches, (ii) phonon velocities are the same for all polarization branches, and, more importantly, (iii) replacement of conventional Debye temperature by a characteristic temperature, θ in the calculations, as described below. The lattice thermal conductivity is now given by

$$K_{\rm lat} = \frac{k_B}{2\pi^2 v}\left(\frac{2\pi k_B T}{h}\right)^3 \times \left[\int_0^x \tau_{\rm tot}\frac{x^4 e^x}{(e^x-1)^2}dx + \frac{\left\{\int_0^x \frac{\tau_{\rm tot}}{\tau_N}\frac{x^4 e^x}{(e^x-1)^2}dx\right\}^2}{\int_0^x \frac{\tau_{\rm tot}}{\tau_U \tau_N}\frac{x^4 e^x}{(e^x-1)^2}dx}\right], \tag{4}$$

where, $x = \frac{\theta(V,T)}{T}$ wherein $\theta(V,T)(\equiv \frac{\hbar\omega}{k_B})$ is the characteristic temperature, h is the Planck constant, ω is the characteristic frequency, and k_B is the Boltzmann constant. The average phonon velocity can be evaluated as follows [30]:

$$v = \left[\frac{1}{3}\left(\frac{2}{v_t^3} + \frac{1}{v_l^3}\right)\right]^{-1/3}, \tag{5}$$

wherein v_l and v_t are the longitudinal and transverse wave velocity, respectively, and are given as

$$v_l = \left(\frac{3B+4G}{3\rho}\right)^{1/2}, \tag{6}$$

$$v_t = \left(\frac{G}{\rho}\right)^{1/2}, \tag{7}$$

where $\rho = \frac{M}{V}$ is the mass density, M is the total atomic mass, B is the bulk modulus, and G is the shear modulus. From Papers I and II, anharmonic computation of V, T-dependent density (≡volume) and elastic moduli helps to evaluate Eqs. (5) through (6) and (7) accurately. The normal and umklapp phonon scattering rates are parametrized in the DC model as [24,31]

$$\frac{1}{\tau_N} = B'\omega^a T^b, \tag{8}$$

$$\frac{1}{\tau_U} = \frac{\hbar\gamma^2(V,T)}{Mv^2\theta(V,T)}\omega^2 T e^{-\theta(V,T)/3T}, \tag{9}$$

where, in Eq. (8), B' ($= 4.4 \times 10^{-11}$ K^{-3}), a ($= 1$), and b ($= 3$) are the fitting parameters. These parameters were chosen such that the computed $K_{\rm lat}$ fits best with the reported datum at RT [18]. Equation (9) is the main equation of the paper through which the contribution from intrinsic anharmonicity can be introduced. For instance, $\gamma(V,T)$ is now explicitly T dependent,

$$\gamma(V,T) = \gamma(V) - \left(\frac{1}{2}mTa(V)\right), \tag{10}$$

where the first term indicates the V-dependent part of γ, whereas the second term depends on T. The details about the V-dependent coefficient $a(V)[\equiv a_0^{'}(\frac{V}{V_0})^m]$ and the values of the anharmonic fitting parameters (m and $a_0^{'}$) involved in it are elaborated in Papers I and II.

Within the textbook definition, Eq. (10) allows one to compute the characteristic temperature to vary with volume and temperature as

$$\theta(V,T) = \theta_0 \exp\left\{-\int_{V_0}^{V}\frac{\gamma(V)}{V}dV\right\} \times \exp\left\{\frac{1}{2}m(m-1)a_0^{'}T\left[\left(\frac{V}{V_0}\right)^m - 1\right]\right\}. \tag{11}$$

In this paper, we have computed θ_0 in Eq. (11) using the relation $\frac{\hbar}{k_B}(\frac{1}{M}\frac{d^2E}{da^2})^{1/2}$ (where E is the total energy and a is the lattice constant), instead of the Debye temperature (θ_D) which is conventionally used in the DC model. The θ_0 corresponds to equilibrium volume at 0 K, zero-pressure condition. The reason for using θ_0 is that the θ_D is computed from the knowledge of P-DOS through first- and second-frequency moments. However, as elaborated in Paper II, the B2 phase of lime is unstable for a considerable range in a (P, T) plane, and may lead to an inaccurate estimation for θ_D. For instance, θ_D calculated from the first- and second-phonon moments of P-DOS is, respectively, 580.41 and 589.19 K for the B1 phase, and 479.29 and 538.28 K for the B2 phase at equilibrium. The θ_0 computed based on self-consistent total energy derivatives circumvents the phonon dynamics at every (P, T) point of interest. Although the θ_0 always remains lower than the θ_D (see Refs. [32–35]), it was demonstrated that θ_0 demarks the low-T quantum region and high-T classical region accurately. It is assumed here that with lower θ, i.e., at the lower characteristic frequency ω, the P-DOS is better represented by ω^2 approximation. However, V and T dependences are still introduced through Eq. (11), where all parameters are optimized from the minimization criterion for Helmholtz free energy that comprises cohesive energy, and QH and anharmonic ion-motional free energies [6,7].

The pressure variation of $K_{\rm lat}$ for the B2 phase is also evaluated using the BTE [1] in the single mode RTA as implemented by the PHONO3PY [36] code. A supercell of size $3 \times 3 \times 3$ and a q-point mesh size of $11 \times 11 \times 11$ is used for the finite displacement method. This scheme, however, is not extended for the B1 phase of CaO since executing the finite displacement technique is found heavy.

Finally, the radiative component of thermal conductivity is determined based on the following relation [4,25]:

$$K_{\rm rad}(T) = \frac{4n^2}{3}\int_0^\infty \frac{1}{\alpha(\vartheta)}\frac{\partial I(\vartheta,T)}{\partial T}d\vartheta, \tag{12}$$

where n is the refractive index, ϑ is the excitation frequency, $\alpha(\vartheta)$ is the frequency-dependent absorption coefficient, and $I(\vartheta,T)$ is the Planck blackbody emission function. The real, $\varepsilon_1(\omega)$, and imaginary, $\varepsilon_2(\omega)$, parts of the dielectric function are computed to derive various optical properties including $\alpha(\vartheta)$ using the standard relations [37]. It is a common practice to solve Eq. (12) by evaluating the dielectric function of the equilibrium volume at ambient condition, and the temperature dependence of $K_{\rm rad}$ is estimated only through $I(\vartheta,T)$. Instead, in this paper, we exploit the results obtained in Papers I and II, and the $\alpha(\vartheta)$ and n both are evaluated at each $V(P,T)$ within the independent particle approximation (IPA) as implemented in the THERMO_PW code [38] in conjunction with the QUANTUM ESPRESSO code [39,40]. The IPA allows the inclusion of single-particle excitations, and the electrons are treated independently of each other when reacting to the external optical perturbation.

III. RESULTS AND DISCUSSION

The equilibrium properties and the volume thermal expansion for the B1 and B2 phases of lime were evaluated using the computed $V_0(T)$, and the results were compared in Papers I and II, respectively. Papers I and II exemplify the role played by phonon anharmonicity while determining various thermal and thermoelastic properties, including the phonon softening at high T. The good comparison of the thermal expansion ensures accurate computation for all the other properties that are derived using them. We note that, in this paper, all figures depicting the computed results are shown as symbols, and the line joining these symbols represents a guide to the eye.

Figure 1 shows the temperature variation of $\gamma[V_0(T)]$ at zero-pressure condition, and represents the measure of vibrational anharmonicity [41]. Thus, $\gamma[V_0(T)]$ represents the combined effect of volume expansion added by T-dependent contribution, the second term in Eq. (10). A common practice among geophysicists is either to fit γ with Eulerian finite volume strain or tune to match the overall conductivity data in Earth's interiors [13,42,43]. Instead, in this paper, $\gamma[V_0(T)]$ is obtained consistently from the *ab initio* calculation added with optimized phonon anharmonicity. In general, γ for both the phases increases with temperature, with a steeper rise for the B1 phase, however. It rises by ∼20% for the B1 phase from 0 to 3000 K. The increase in γ is attributed to the closed-packed structures and can be explained by the nature of the anharmonicity. Stacey and Issak [44] have demonstrated that

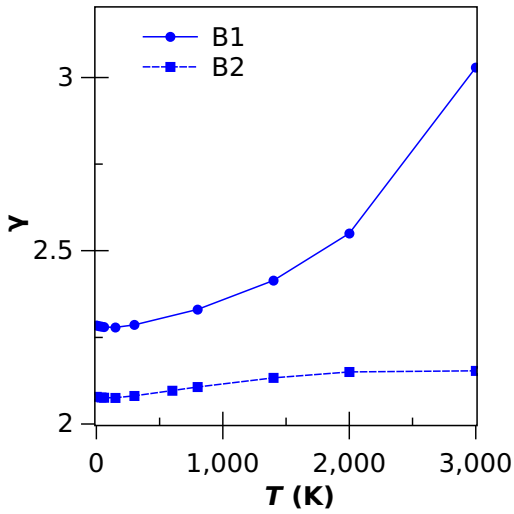

FIG. 1. Grüneisen parameter as a function of temperature at ambient pressure.

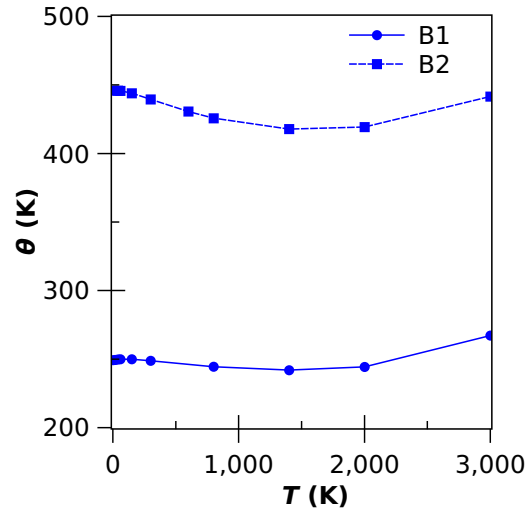

FIG. 3. Characteristic temperature as a function of temperature at ambient pressure.

closed-packed structure with bonds to each atom are always appearing opposite in pairs; i.e., they are symmetrical, for which the phonon anharmonic contribution lowers the value of C_V with temperature [6,7,32–35]. In cubic structure, although the thermal expansion of the crystal lowers the phonon frequency but with positive anharmonicity, so as to restrict the overwhelming thermal expansion for the case of lime [6,7], it reduces the rate of phonon softening. The B2 phase is dynamically unstable at high-T and zero-pressure conditions; the phonon states contributing to the thermal gamma are less in number. This explains the lower value of γ for the B2 phase. The variation of γ with pressure at fixed temperatures is shown in Fig. 2. The structural phase diagram of lime, presented in Paper II, predicts the triple point (TP; coexistence of B1, B2, and liquid phase) at 23 GPa and 4600 K. Thus, the TP corresponds to the LM region having the highest temperature and lowest pressure and thus provides the most stringent test to measure the largest possible anharmonicity that can be found in the entire Earth's LM. Hence, for Fig. 2 and all the other computed P-dependent properties, one of the temperatures we have chosen is the temperature corresponding to the TP, i.e., 4600 K for both the B1 and B2 phases of CaO. One fixed temperature chosen for both phases is a temperature below the TP and close to normal T_M, i.e., 3000 K, where the B1 phase is stable but with the largest anharmonicity. Apart from these two temperatures, we have also evaluated all the properties at the temperature corresponding to the CMB, i.e., 3800 K. Experimental T_M for the B1 phase is 3160 K [45] whereas classically simulated T_M for the B2 phase is 2605 K (see the Supplemental Material of Paper II). The structural phase diagram in Paper II predicts a negative melting slope beyond 140 GPa and 7800 K. To investigate the properties at this transition point (from a pressure viewpoint, this lies in the vicinity of the CMB), where the B2 phase is stable and is in competition with the denser liquid phase [7], we extend the computation for the B2 phase close to this pressure and beyond. In Fig. 2, altogether, γ decreases with pressure. The γ at $(P, T) = (0\ \text{GPa}, 3000\ \text{K})$ for both the phases almost coincides but that of (0 GPa, 4600 K) has 5% variation. For 3800 K, the γ of the B1 and B2 phases coincides with that of the 3000 K data, specifically at higher pressures. The rate of decrease of γ is more for the B1 phase. Since with pressure the anharmonicity is suppressed, eventually the results for γ converge to their respective values.

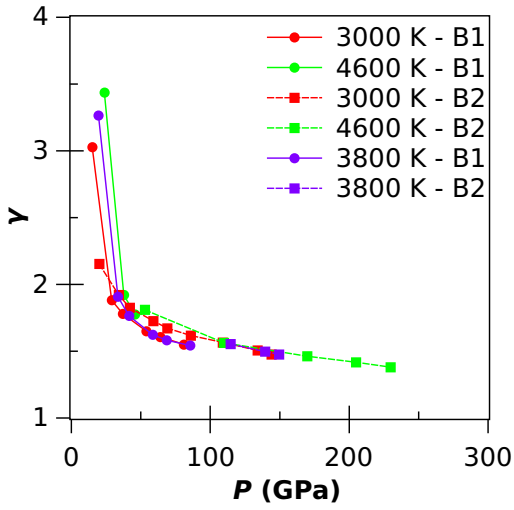

FIG. 2. Grüneisen parameter as a function of pressure.

The characteristic temperature, $\theta(V,T)$, is one of the crucial characteristics of a material, which reflects its structural stability, the strength of bonds between its elements, and its density [41]. Figure 3 shows the temperature variation of $\theta[V_0(T)]$ that is evaluated by including the anharmonic contribution using Eq. (11). At 0 K and zero pressure, θ_0 of both the phases varies by 35% and at 3000 K the variation is 37%. Initially, θ decreases with an increase in temperature but increases beyond 2000 K. The zero-pressure increase in $\theta[V_0(T)]$ reflects the dominating T-dependent contribution. The P-dependent $\theta(V,T)$ is shown in Fig. 4. The P-dependent behavior of θ is opposite to that of T-dependent nature. For

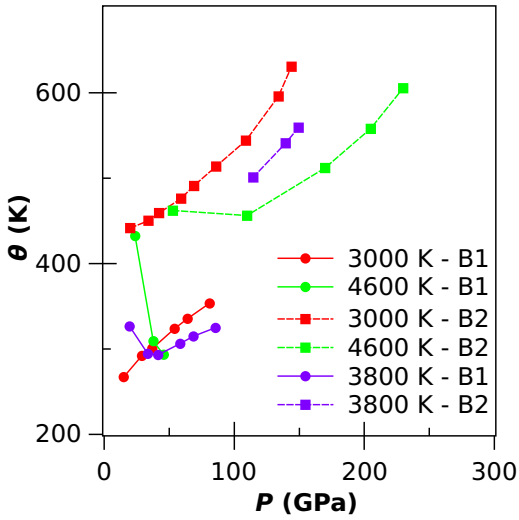

FIG. 4. Characteristic temperature as a function of pressure.

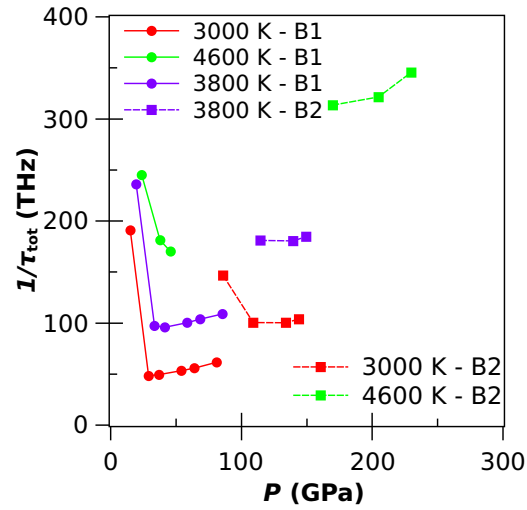

FIG. 6. Total phonon scattering rate as a function of pressure.

3000 K, θ of the B1 phase increases gradually with pressure but at $P \sim 50$GPa it shows a downward trend. It is due to the fact that at $T = 3000$ K, B1-CaO transforms to B2 phase for $P \geqslant 50$ GPa. For 4600 K, temperature dominates the pressure for a studied range, and θ in the B1 phase decreases. For the B2 phase, θ increases with pressure for all temperatures. The θ for 3800 K of the B1 phase initially decreases and then increases beyond 50 GPa and that of the B2 phase mimics the trend of the other two temperatures and it increases throughout the investigated pressure window. Within the same phase, a dispersion in θ for different temperatures accounts for the anharmonicity.

The temperature dependence of the total phonon scattering rate, $\frac{1}{\tau_{\text{tot}}}$, is shown in Fig. 5. For both the phases, $\frac{1}{\tau_{\text{tot}}}$ increases with temperature and shows a dispersion beyond 500 K. Throughout the temperature range, the scattering rate of the B2 phase remains higher in magnitude than the B1 phase, indicating that the heat flux due to phonons increases

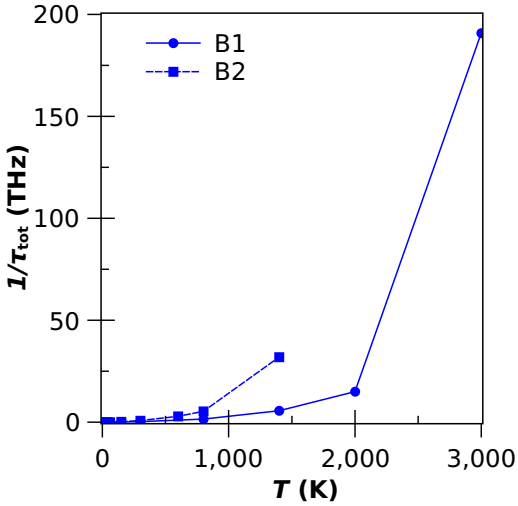

FIG. 5. Total phonon scattering rate as a function of temperature at ambient pressure.

rapidly for the B2 phase. In our previous papers [6,7], we have demonstrated the sensitivity of the expanded and compressed volumes on the PDC and P-DOS for B1-CaO, particularly at the Γ point of the Brillouin zone. Due to the increase of frequency gap induced by LO-TO splitting, the three-phonon scattering rate of CaO increases rapidly. Comparatively, the B2 phase shows less sensitivity to the compressive strain. As elaborated in Ref. [8] for the case of CaO, the third-order anharmonic scattering rate (≡reciprocal of phonon frequency) decreases with phonon frequency at ambient conditions. But it should increase with temperature. This assertion is based on Papers I and II which illustrate that the anharmonic frequency softens with temperature, and hence the scattering rate increases. Due to the negative shear modulus [7] for the B2 phase at zero-pressure condition, the results for $\frac{1}{\tau_{\text{tot}}}$ are restricted below 1500 K. The P-dependent total phonon scattering rate is shown in Fig. 6. Again, the shear stability criteria restrict the data points in Fig. 6. Except for the B2 phase, for 4600 K, the $\frac{1}{\tau_{\text{tot}}}$ initially decreases with pressure but then shows an upward trend.

Figure 7 shows the temperature variation of K_{lat} at zero-pressure condition. The K_{lat} for both the phases increases initially, attains a peak value, and then decreases with an increase in temperature. Computed results are compared with the RT datum due to Yang *et al.* [18], Knoop *et al.* [46], and the recent high-T first-principles calculations due to Ma *et al.* [8]. Ma *et al.* [8] have solved the BTE using the third-order force constant and derived the lattice thermal conductivities up to 3000 K at atmospheric pressure. Our results of the temperature variation of K_{lat} coincide with the results in Ref. [8]. The trend of the computed K_{lat} is also validated with the available thermal conductivity of the isostructural and similar alkaline oxide, MgO [13–16]. The experimental value of K_{lat} at 300 K is scattered for MgO, ranging from 36 to 70 $\text{W m}^{-1}\,\text{K}^{-1}$ [13], whereas the computed RT K_{lat} of CaO and other reported data is around 20 $\text{W m}^{-1}\,\text{K}^{-1}$. Further, the trend of K_{lat} obtained for CaO beyond the peak value is the same as that for the complete alkaline-earth oxides family [8,13–16], i.e., as the temperature increases, the K_{lat} decreases. The decrease in K_{lat} is related to the phonon

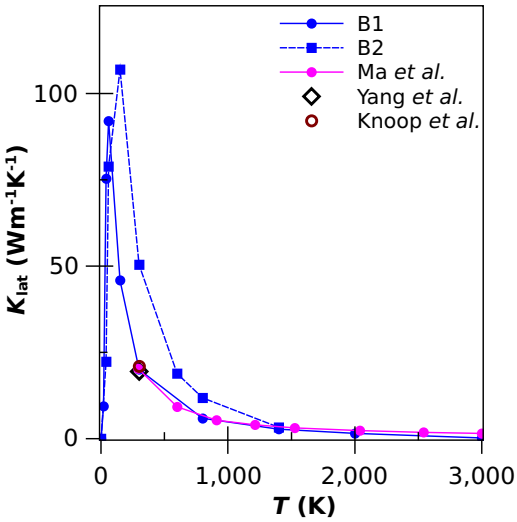

FIG. 7. Lattice thermal conductivity as a function of temperature at ambient pressure. The pink circle with a line and the diamond symbol are the BTE based results due to Ma *et al.* [8] and Yang *et al.* [18], respectively, for the B1 phase of CaO. The open circle is the *ab initio* Green-Kubo based result due to Knoop *et al.* [46] for the B1 phase of CaO.

softening [6,7] and hence to the decrease in group velocities. For the B1 and B2 phases, K_{lat} sharply increases up to 60 and 150 K, respectively, starts decreasing, and approaches zero at higher temperatures. The low-T region is governed by the normal process, Eq. (3). Traditionally the DC model utilizes the QH inputs in Eq. (4) through (11), whereas in this paper, we utilized all parameters which are derived after including the explicit effect of temperature. The variation of K_{lat} with pressure at different temperatures is shown in Fig. 8. In a similar study, Ma *et al.* [8] have calculated high-P conductivities for alkaline-earth oxides including the CaO

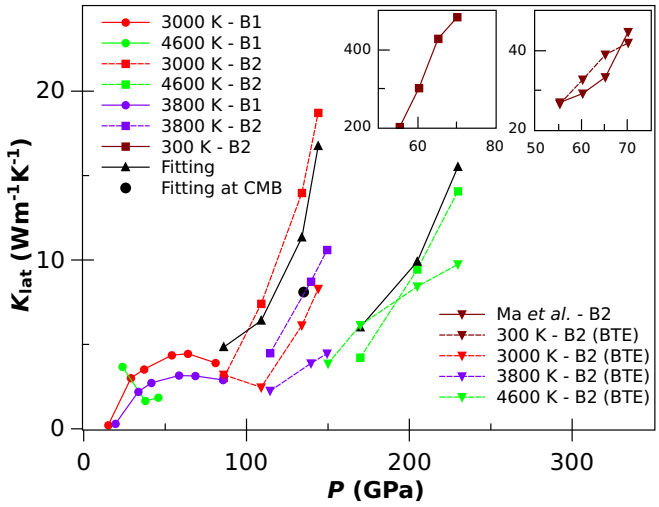

FIG. 8. Lattice thermal conductivity as a function of pressure. The fitting of the data is done using the equation $\frac{K_{lat}(P,T)}{K^0_{lat}} = (\frac{V_0}{V})^g(\frac{T_0}{T})^{\beta'}$. The compared BTE based result due to Ma *et al.* [8] is for the B2 phase of CaO.

but at RT. The present BTE based results at 300 K for the B2 phase agree reasonably with the reported results [8] (inset of Fig. 8). It is to be noted that the difference in these two sets of observations is assigned to the different compressed volumes utilized to determine the pressure variation of K_{lat}, and to the size of the supercells. For example, the present computation is based on the volume corresponding to a given pressure after finding the equilibrium volume at each temperature, $V_0(T)$, as derived in Papers I and II. Figure 8 infers that the DC model based results generally remain higher. We investigated this systematic deviation, and it is attributed to the higher value for the characteristic temperature of the B2 phase, Fig. 3. The larger value of the characteristic temperature governs the magnitude of the K_{lat}. The results in Ref. [8] show the general trend which is similar to the present estimates, i.e., slightly downward bending with pressure for the B1 phase, but the concave-up trend for the B2 phase. The overall trend of the pressure variation of K_{lat} for CaO is similar to that of MgO [13–16], except for the difference in magnitude. As reported in Ref. [15], the K_{lat} at 300 K increases with an increase in temperature. The K_{lat} of 3000, 3800, and 4600 K of the B2 phase increases in a similar manner but with a steeper slope while that of the B1 phase also increases. This is true for both DC-model and BTE based findings. Since the present investigation aims to examine the K_{lat} at Earth's LM and core conditions, temperature is kept $3000 < T < 4600$ K. At this temperature range and with a pressure ∼140 GPa, Paper II reveals the phase transitions between B1, B2, and the liquid phase of lime. These intrinsic phenomena govern the behavior of K_{lat}, and its discussion is in order. For 3000 K of the B1 phase, K_{lat} increases up to 50 GPa and then decreases. This tendency is similar to the high-P results for K_{lat} in MgPv and Mg bridgmanite (Mg-Brg) [3]. The increase in K_{lat} is attributed to the increase in phonon frequency [6,7] and hence to the increase in group velocities, and to the lattice quasiparticle longer lifetimes. In their rigorous investigation, Ma *et al.* [8] have also noted that the effect of specific heat and high-frequency optical modes is less due to the variation of K_{lat} with volume but the group velocity is an important parameter. The downward trend with pressure for the B1 phase of CaO is due to phase instability. Ma *et al.* [8] have also noted that close to and at the phase transition, K_{lat} decreases for a given phase. However, within the stability limit for the B1 phase, K_{lat} increases. For 4600 K, due to the strong temperature effect, the value of K_{lat} decreases at low P, but at higher pressure, the anharmonicity is suppressed and K_{lat} starts increasing. For the stable B2 phase, a uniform increasing trend is observed. Though the K_{lat} increases with pressure, the rate of increase reduces with temperature. Further, at higher temperatures, K_{lat} will attain a lower value at a fixed pressure. A similar trend was obtained in the recent *ab initio* studies by Dekura and Tsuchiya [9] for MgPv and Mg-Brg, and also by Zhang *et al.* [3] for MgPv, Mg-Brg, and CaPv. The high-P variation of K_{lat} for CaPv increases monotonically up to 170 GPa [3] similar to the B2 phase of CaO. It is important to note that K_{lat} for MgPv, Mg-Brg, and CaPv under mantle and core conditions is of comparable magnitude to that of the B2-CaO. To interpret the DC-model data, we attempt to fit K_{lat} results for the B2 phase using a frequently

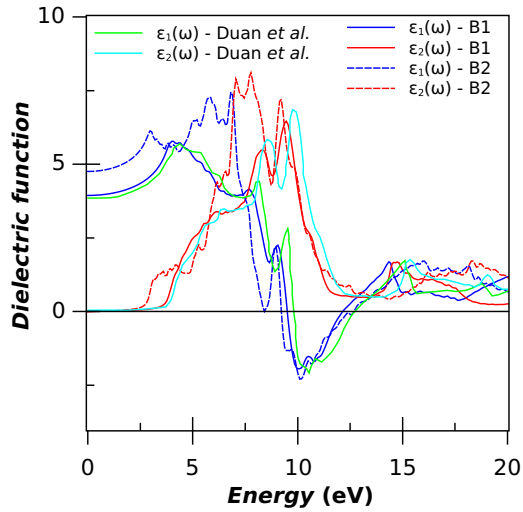

FIG. 9. Real and imaginary parts of the frequency-dependent dielectric functions. The compared results are the first-principles calculations due to Duan *et al.* [48].

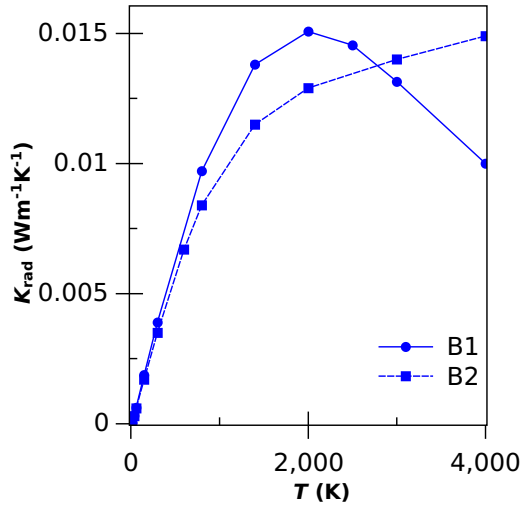

FIG. 10. Radiative thermal conductivity as a function of temperature at ambient pressure.

employed power law, $\frac{K_{lat}(P,T)}{K^0_{lat}} = (\frac{V_0}{V})^g(\frac{T_0}{T})^{\beta'}$, where 0 super- and subscripts refer to the reference equilibrium condition, i.e., volume $V_0(T_0)$ and temperature ($T_0 = 300$ K), and the power coefficients g and β' are selected to find an overall fit to the derived data points. We can reasonably fit (lines with black symbols in Fig. 8) 3000, 3800, and 4600 K data points with V- and T-dependent $g(V,T) = 3\gamma(V,T) + 2q(V,T) - \frac{1}{3}$, where the log-derivative of $\gamma(V,T)$, Eq. (10), is computed by $q(V,T) = -\frac{V}{\gamma(V,T)}\frac{d\gamma(V,T)}{dV}|_{T_0} - \frac{1}{\gamma(V,T)}\{\frac{1}{2}m^2Ta_0'(\frac{V}{V_0})^m\}$, whereas $\beta'(= 1.351)$ is considered as a constant fitting parameter. The value of the only fitting parameter β' [as g and q are computed at a given (V, T) point] different than the unity is also reported in the literature [16]. It is noteworthy that since the present findings involve the computation of K_{lat} through the anharmonic inputs to the DC model, we find the parameter g to be dependent on pressure and temperature via $\gamma(V,T)$ and $q(V,T)$ in a self-consistent manner. A similar exercise can be adopted for BTE based results also. The anharmonic DC model predicts K_{lat} at the CMB ($T\sim$3800 K, $P\sim$135 GPa) to be 8 W m^{-1} K^{-1}, whereas the BTE prediction is 4.9 W m^{-1} K^{-1} at the CMB. This value is close to (in W m^{-1} K^{-1}) $K_{lat}^{Mg-Brg} \sim 4.3$, $K_{lat}^{Mg-Brg} \sim 6.3$, and $K_{lat}^{CaPv} \sim 13$ [3], all estimated at the CMB.

A vital component to compute K_{rad} is the absorption coefficient. As discussed in the Introduction, all the optical properties of a material can be derived from $\varepsilon_1(\omega)$ and $\varepsilon_2(\omega)$ within the IPA [47]. However, it is necessary to validate the variation of $\varepsilon_1(\omega)$ and $\varepsilon_2(\omega)$ with the excitation energy at different pressures (≡volumes). We have presented the results for $\varepsilon_1(\omega)$ and $\varepsilon_2(\omega)$ for both the phases at their respective equilibrium volumes, and compared the B1 phase results with the available data [48] in Fig. 9. The computed results agree well with the reported data with the principal peak for $\varepsilon_2(\omega)$ at 9.46 eV and the principal dip for $\varepsilon_1(\omega)$ at 10.02 eV. No comparison for the B2 phase is available. However, a mutual comparison between the B1 and B2 phases reveals that the entire optical response for the B2 phase shifts towards the lower excitation energy. The real part of the dielectric function shows a similar response at low (comparable to the average phonon energy) excitation energy for both structures but with a higher value for the B2 phase. The long wavelength limit $\varepsilon_1(\omega \to 0)$ value is 20% higher for the B2 phase. This explains the higher refractive index (= 2.16) of the B2 phase. At this low excitation energy range, the absorption as measured by $\varepsilon_2(\omega)$ is zero. The B2 phase shows two major peaks in $\varepsilon_2(\omega)$: one close to 7.5 eV and the other at ∼9.5 eV. The calculated principal peaks for $\varepsilon_2(\omega)$ shifts to lower photon energy but the principal dip for $\varepsilon_1(\omega)$ remains the same as that of the B1 phase. Since the present paper aims to study the (P, T) variation of K_{rad}, we have computed $\varepsilon_1(\omega)$ and $\varepsilon_2(\omega)$ (results are not shown here) at respective $V(T)$, and our observations are as follows. Though the overall nature of $\varepsilon_1(\omega)$ and $\varepsilon_2(\omega)$ remains the same, both graphs shift to a higher frequency side. However, the results for $\varepsilon_1(\omega)$ and $\varepsilon_2(\omega)$ show larger modulation for compressed volume corresponding to 100 GPa for the B1-CaO compared to the B2 phase. The refractive index systematically increases (decreases) to compressed (expanded) volumes. The magnitude of the refractive index determines the magnitude of K_{rad}, Eq. (12).

Figure 10 shows the temperature variation of K_{rad} at zero-pressure condition. The results for K_{rad} remain two orders of magnitude smaller than K_{lat} for the highest temperature studied in the paper. For the B1 phase, K_{rad} increases up to 2000 K and then decreases, whereas for the B2 phase, the K_{rad} increases for the entire temperature range. Commonly, Eq. (12) is used to compute K_{rad} with $\alpha(\vartheta)$ and n evaluated at equilibrium condition. This procedure has shown (results are not shown here) a monotonous increase in K_{rad} for the B1 phase. Thus, the IPA approach adopted to compute the optical response at respective volumes capture the effect of (P, T) adequately. The pressure variation of K_{rad} is shown in Fig. 11. For both the phases up to 4600 K, the K_{rad} increases until the pressure is 23 GPa and then decreases monotonically. However, for the B1 phase at higher temperatures, the unstable phonons restrict the calculation to moderate pressures.

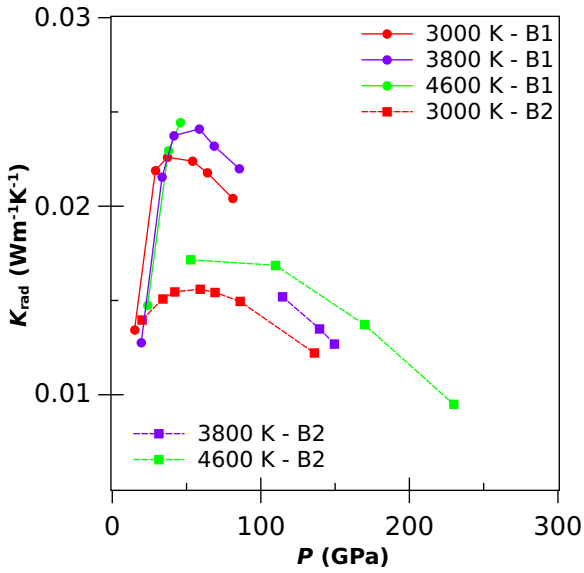

FIG. 11. Radiative thermal conductivity as a function of pressure.

IV. DISCUSSION

Thermal conductivity is a nonharmonic property of materials. In this paper, the phonon anharmonicity added and DFT-assisted DC approach is utilized to examine the $P-T$ dependence of lattice thermal conductivity, and discussed in reference to the BTE based findings. First-principles calculations in combination with the QH and anharmonic contribution to the vibrational properties were carried out to find input parameters to the DC model, such as the characteristic temperature, average phonon group velocity, and Grüneisen parameter. The anharmonic interatomic force constants, which are vital to give accurate lattice thermal conductivity, usually require a relatively large supercell to include the long-range interactions, which are peculiar to polarized and anharmonic systems like lime [49]. For instance, the results for $K_{\rm lat}$ of B2-CaO computed by Ma *et al.* [8] with a $4\times4\times4$ supercell and the present paper with a $3\times3\times3$ supercell show a similar trend to each other but are slightly different in magnitude. For B1-CaO, the $3\times3\times3$ supercell has 54 atoms but for $4\times4\times4$, it increases to 128. Thus, obtaining the higher-order force constants to find converged transport properties is progressively a computationally heavy task with higher-dimension supercells. The effect of the inclusion of a third-order force constant in lattice dynamics, in general, is to renormalize the phonon frequencies, and hence is reflected in all the other physical properties. We have incorporated the anharmonicity directly into the computation of the Helmholtz free energy by employing the lowest-order TPT. We can interpret the effect of the cubic force constant on the phonon frequencies as follows. For instance, as elaborated by Eq. (6) of Paper I, we can expand the phonon frequency in the V,T plane as $\omega_{n,\vec{q}}(V,T)\approx\omega^{QH}(V,T_0)+\{\frac{1}{\omega_0}\frac{\partial\omega(V_0,\,T)}{\partial T}\}\omega_0 T$, with $(\frac{\partial\,\ln\omega(V,T)}{\partial T})_{V_0}\equiv a_0^{'}(\frac{V}{V_0})^m$. Here, ω_0 are the phonon frequencies at equilibrium. The phonon branch index $(n,\vec{q})$ is omitted on the right-hand side only for convenience. A superscript QH denotes quasiharmonic calculations at reference temperature $T_0(=1\ \mathrm{K})$. The second term is explicitly T dependent. Thus, the TPT approximation modifies the QH phonon dynamics through anharmonic parameters, and to a good approximation, it can be considered like the phonon-renormalization-frequency approach. Accurate thermal expansion justifies the proper inclusion of the three-phonon anharmonic interactions. This approach not only reduced the computational cost [6,7] but also yielded a good result for low-P temperature variation of lattice and radiative thermal conductivities. This is evident from the comparison made in Fig. 7. We also tested various combinations for DC-model parameters $a=1$ and $b=3$ in Eq. (8). Within a reasonable range of a and b, the normal scattering is negligible with respect to the umklapp scattering and hence plays no role in Eq. (4). This observation suggests that the normal relaxation time $(\frac{1}{\tau_N})$ varies linearly with phonon frequency, and follows the Debye law in temperature. The results and discussion for pressure variation of $K_{\rm lat}$ utilize the self-consistent thermodynamic model with the no fitting parameter. The pressure variation of lattice conductivity for the B2 phase by the DC model deviates from the BTE based approach, Fig. 8. Nevertheless, the gross behavior in both sets of data is similar. The large estimate for $K_{\rm lat}$ is due to the large characteristic temperature for B2-CaO. Since the characteristic temperature is related to the phonon sound velocities [it demands the use of full lattice dynamics at every $(P,\ T)$ point for accurate calculations], the third-order BTE based results are more reliable. For instance, in a recent paper, Ma *et al.* [8] have also emphasized the accurate determination of group velocity and phonon lifetime for accurate calculation of $K_{\rm lat}$. The magnitude of radiative thermal conductivity is two orders lower than that of the lattice thermal conductivity, and hence, the total thermal conductivity retains the magnitude of the lattice thermal conductivity. This is in contrast to Mg- and Ca based perovskites [3], where at high-T,P conditions, the contribution from $K_{\rm rad}$ is vital. The computed results can be used to find the heat flux (q) from the core to mantle across the CMB using Fourier's law for heat conduction $q=-K_{\rm lat}\nabla T$ and from the knowledge of the geotherm.

V. CONCLUSION

Overall, the anharmonic-parameters motivated DC model and the BTE approach are proved to be efficient tools to compute the temperature and pressure variation of lattice thermal conductivity of quicklime, though, one expects a large modulation in acoustic phonons at compressed volumes, and its effect should be incorporated into the calculations. In the present form of the DC model, the input quantities are derived at the anharmonic level. As an attractive feature of the computational scheme, the characteristic temperature derived from the second-order derivative of the total energy circumvents the calculation of the Debye temperature from the phonon frequency moments at every $(P,\ T)$ point. Formally, the lowest-order TPT to account for the phonon anharmonicity is similar to renormalizing the phonon frequencies, and accurate results for thermal expansion [6,7] and lattice conductivity at high T and low P is an indication of proper inclusion of the three-phonon interaction. Thus, the overestimated results at higher pressures due to the DC model can be rectified by formulating $K_{\rm lat}$ that includes the effect of the complete PDC. We

further propose that the BTE calculation for $K_{\rm lat}(P,T)$ should be based on accurate $V_0(P,\ T)$. Although the $K_{\rm rad}$ is negligible at P and T relevant to the LM and core, it is to be noted that the $K_{\rm lat}$ and therefore the heat flux across the CMB for B2-CaO is of the same order and compatible to that of the Mg based oxides and perovskite, along with the CaPv. This justifies the study of high-P, T findings for the thermal conductivity of quicklime in the B2 phase, and invites further exploration either from *ab initio* simulations or by experiments.

ACKNOWLEDGMENTS

The high-performance computing facility at the Department of Physics, Maharaja Krishnakumarsinhji Bhavnagar University, under Grant No. PGP/UGC12/73F/2019 of the University Grants Commission, New Delhi, India, is greatly acknowledged. The authors are grateful to the reviewers for suggesting valuable improvement points to the study.

[1] J. M. Ziman, *Electrons and Phonons: The Theory of Transport Phenomena in Solids* (Oxford, New York, 2001).
[2] Y. Wang, Z. Lu, and X. Ruan, J. Appl. Phys. **119**, 225109 (2016).
[3] Z. Zhang, D.-B. Zhang, K. Onga, A. Hasegawa, K. Ohta, K. Hirose, and R. M. Wentzcovitch, Phys. Rev. B **104**, 184101 (2021).
[4] A. F. Goncharov, B. D. Haugen, V. V. Struzhkin, P. Beck, and S. D. Jacobsen, Nature (London) **456**, 231 (2008).
[5] A. M. Hofmeister, Science **283**, 1699 (1999).
[6] P. Vyas, A. B. Patel, and N. K. Bhatt, Physica B **645**, 414250 (2022).
[7] P. Vyas, A. B. Patel, and N. K. Bhatt, Phys. Rev. B **107**, 014107 (2023); **107**, 139903(E) (2023).
[8] Y. Ma, S. Yang, K. He, and C. Lu, Comput. Mater. Sci. **210**, 111446 (2022).
[9] H. Dekura and T. Tsuchiya, Geophys. Res. Lett. **46**, 12919 (2019).
[10] N. Ghaderi, D. B. Zhang, and H. Zhang, Sci. Rep. **7**, 5417 (2017).
[11] F. Yang, Q. Zeng, B. Chen, D. Kang, S. Zhang, J. Wu, X. Yu, and J. Dai, Chin. Phys. Lett. **39**, 116301 (2022).
[12] V. Haigis, M. Salanne, and S. Jahn, Earth Planet. Sci. Lett. **355**, 102 (2012).
[13] N. de Koker, Earth Planet. Sci. Lett. **292**, 392 (2010).
[14] X. Tang and J. Dong, Proc. Natl. Acad. Sci. USA **107**, 4539 (2010).
[15] S. Imada, K. Ohta, T. Yagi, K. Hirose, H. Yoshida, and H. Nagahara, Geophys. Res. Lett. **41**, 4542 (2014).
[16] D. A. Dalton, W. P. Hsieh, G. T. Hohensee, D. G. Cahill, and A. F. Goncharov, Sci. Rep. **3**, 2400 (2013).
[17] T. Fan and A. R. Oganov, Comput. Phys. Commun. **266**, 108027 (2021).
[18] Z. Yang, K. Yuan, J. Meng, X. Zhang, D. Tang, and M. Hu, Nanotechnology **32**, 025709 (2020).
[19] P. K. Schelling, S. R. Phillpot, and P. Keblinski, Phys. Rev. B **65**, 144306 (2002).
[20] A. J. H. McGaughey and M. Kaviany, Adv. Heat Transfer **39**, 169 (2006).
[21] D. A. McQuarrie, *Statistical Mechanics* (University Science Books, Melville, NY, 2000).
[22] A. Fiorentino and S. Baroni, Phys. Rev. B **107**, 054311 (2023).
[23] J. Callaway, Phys. Rev. **113**, 1046 (1959).
[24] Y. Zhang, J Materiomics **2**, 237 (2016).
[25] H. Keppler, L. S. Dubrovinsky, O. Narygina, and I. Kantor, Science **322**, 1529 (2008).
[26] P. Vyas, N. K. Bhatt, and P. R. Vyas, AIP Conf. Proc. **2352**, 020060 (2021).
[27] A. Erba, M. Shahrokhi, R. Moradian, and R. Dovesi, J. Chem. Phys. **142**, 044114 (2015).
[28] G. A. Slack, Solid State Phys. **34**, 1 (1979).
[29] D. T. Morelli and G. A. Slack, *High Lattice Thermal Conductivity Solids* (Springer, New York, NY, 2006).
[30] H. Wangqiang, H. Houbing, L. Zhuhong, and M. Xingqiao, Chin. Phys. B **27**, 016201 (2018).
[31] R. Berman, *Thermal Conduction in Solids* (Oxford University Press, Oxford, 1976).
[32] D. D. Satikunvar, N. K. Bhatt, and B. Y. Thakore, J. Appl. Phys. **129**, 035107 (2021).
[33] R. H. Joshi, B. Y. Thakore, P. R. Vyas, A. R. Jani, and N. K. Bhatt, Chin. Phys. B **26**, 116502 (2017).
[34] N. K. Bhatt, A. R. Jani, P. R. Vyas, and V. B. Gohel, Physica B (Amsterdam, Neth.) **357**, 259 (2005).
[35] N. K. Bhatt, B. Y. Thakore, P. R. Vyas, and A. R. Jani, Physica B (Amsterdam, Neth.) **405**, 3492 (2010).
[36] A. Togo, L. Chaput, and I. Tanaka, Phys. Rev. B **91**, 094306 (2015).
[37] H. Mei, Y. Zhong, P. Wang, Z. Jia, C. Li, and N. Cheng, Materials **11**, 449 (2018).
[38] https://dalcorso.github.io/thermo_pw/.
[39] P. Giannozzi, S. Baroni, N. Bonini, M. Calandra, R. Car, C. Cavazzoni, D. Ceresoli, G. L. Chiarotti, M. Cococcioni, I. Dabo, A. Dal Corso, S. Fabris, G. Fratesi, S. de Gironcoli, R. Gebauer, U. Gerstmann, C. Gougoussis, A. Kokalj, M. Lazzeri, L. Martin-Samos *et al.*, J. Phys.: Condens. Matter **21**, 395502 (2009).
[40] P. Giannozzi, O. Andreussi, T. Brumme, O. Bunau, M. Buongiorno Nardelli, M. Calandra, R. Car, C. Cavazzoni, D. Ceresoli, M. Cococcioni, N. Colonna, I. Carnimeo, A. Dal Corso, S. de Gironcoli, P. Delugas, R. A. DiStasio, Jr., A. Ferretti, A. Floris, G. Fratesi, G. Fugallo *et al.*, J. Phys.: Condens. Matter **29**, 465901 (2017).
[41] N. Ashcroft and N. Mermin, *Solid State Physics* (Saunders College Publishing, Fort Worth, 1976).
[42] L. Stixrude and C. Lithgow-Bertelloni, Geophys. J. Int. **162**, 610 (2005).
[43] M. Delannoy and G. Perrin, J. Phys. Chem. Solids **41**, 11 (1980).

[44] F. D. Stacey and D. G. Isaak, J. Geophys. Res. **108**, 2440 (2003).
[45] T. Bgasheva, T. Falyakhov, S. Petukhov, M. Sheindlin, A. Vasin, and P. Vervikishko, J. Am. Ceram. Soc. **104**, 3461 (2021).
[46] F. Knoop, T. A. R. Purcell, M. Scheffler, and C. Carbogno, Phys. Rev. Lett. **130**, 236301 (2023).
[47] H. Ahmad, A. Rauf, A. Ahmad, A. Ulhaq, and S. Muhammad, RSC Adv. **11**, 32330 (2021).
[48] Y. Duan, L. Qin, G. Tang, and L. Shi, Eur. Phys. J. B **66**, 201 (2008).
[49] B. B. Karki and R. M. Wentzcovitch, Phys. Rev. B **68**, 224304 (2003).